J. Fluid Mech. (1996), *vol.* 311, *pp.* 327–343
Copyright © 1996 Cambridge University Press

Simple shearing flow of a dry Kelvin soap foam

By DOUGLAS A. REINELT[1] AND ANDREW M. KRAYNIK[2]

[1] Department of Mathematics, Southern Methodist University, Dallas, TX 75275-0156, USA

[2] Engineering Sciences Center, Sandia National Laboratories, Albuquerque, NM 87185-0834, USA

(Received 27 June 1995 and in revised form 8 November 1995)

Simple shearing flow of a dry soap foam composed of identical Kelvin cells is analysed. An undeformed Kelvin cell has six planar quadrilateral faces with curved edges and eight non-planar hexagonal faces with zero mean curvature. The elastic-plastic response of the foam is modelled by determining the bubble shape that minimizes total surface area at each value of strain. Computer simulations were performed with the Surface Evolver program developed by Brakke. The foam structure and macroscopic stress are piecewise continuous functions of strain. Each discontinuity corresponds to a topological change (T1) that occurs when the film network is unstable. These instabilities involve shrinking films, but the surface area and edge lengths of a shrinking film do not necessarily vanish smoothly with strain. Each T1 reduces surface energy, results in cell-neighbour switching, and provides a film-level mechanism for plastic yield behaviour during foam flow. The foam structure is determined for all strains by choosing initial foam orientations that lead to strain-periodic behaviour. The average shear stress varies by an order of magnitude for different orientations. A Kelvin foam has cubic symmetry and exhibits anisotropic linear elastic behaviour; the two shear moduli and their average over all orientations are $G_{min} = 0.5706$, $G_{max} = 0.9646$, and $\overline{G} = 0.8070$, where stress is scaled by $T/V^{1/3}$, T is surface tension, and V is bubble volume. An approximate solution for the microrheology is also determined by minimizing the total surface area of a Kelvin foam with flat films.

1. Introduction

Soap foams are highly structured fluids in which polyhedral gas bubbles are separated by a continuous network of thin liquid films that are stabilized against rupture by the presence of surfactants. Applications and early studies of foam flow have been reviewed by Kraynik (1988). The structure of a dry foam under static conditions consists of individual films with surface tension T and uniform mean curvature. The volume fraction of continuous liquid phase is zero in the dry limit; Plateau border channels that form along cell edges in wet foams are absent. The shape of each film satisfies the Young-Laplace equation

$$\Delta p_k = 2\,T\,(\nabla \cdot \boldsymbol{n}_k) \tag{1.1}$$

where Δp_k is the pressure difference between adjacent bubbles separated by film k, $\boldsymbol{n}_k$ is a local unit vector normal to film k, and the term in parentheses is the sum of the principal curvatures. The factor of 2 accounts for both film interfaces. To balance

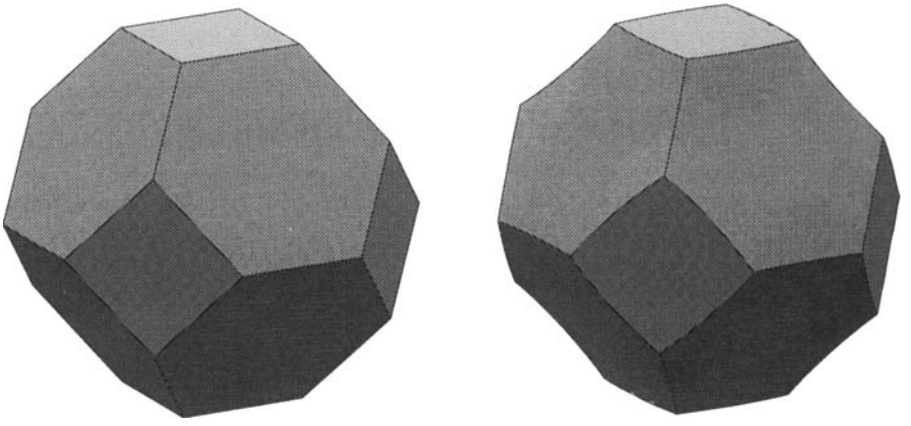

FIGURE 1. The regular tetrakaidecahedron on the left has fourteen flat faces: six squares and eight regular hexagons. The Kelvin cell on the right has flat quadrilateral faces and non-planar hexagonal faces with zero mean curvature. The quadrilateral faces for both polyhedra are perpendicular to the x-, y-, and z-axes in the reference orientation.

forces and minimize surface energy, three films intersect along cell edges at equal dihedral angles of 120° and four edges meet at each vertex at equal tetrahedral angles of $\cos^{-1}(-1/3)$. These equilibrium conditions were recognized by Plateau (1873). Taylor (1976) has shown that Plateau's laws are a mathematical consequence of minimizing surface area – a requirement of stable foam structures (see also Almgren & Taylor 1976).

The regular tetrakaidecahedron shown in figure 1 packs to fill space. Two regular hexagons and a square meet along each edge. The two hexagons join at the tetrahedral angle 109.47° and the dihedral angle between each hexagon and square is 125.26°. This structure possesses the film-network topology that is necessary to satisfy equilibrium: three films meet at each edge and four edges meet at each vertex; however, this structure does not have the necessary equal dihedral angles.

Kelvin (1887) recognized that an equilibrium foam structure could be achieved by distorting the faces of the planar tetrakaidecahedron so that they meet at 120°; all vertex angles would then be equal to the tetrahedral angle. Each film has zero mean curvature and satisfies the nonlinear partial differential equation based on (1.1) corresponding to $\Delta p_k = 0$. A single bubble in the equilibrium foam structure is known as Kelvin's minimal tetrakaidecahedron or a Kelvin cell and is shown in figure 1 next to the regular tetrakaidecahedron. The squares become planar quadrilateral faces with curved edges and the hexagons become non-planar saddle surfaces with zero mean curvature. Even though planar films have zero mean curvature, no foam *in equilibrium* can be composed entirely of flat films because no polygon with straight edges has all vertex angles equal to the tetrahedral angle.

Kelvin determined an approximate analytical solution for the curved faces. Accurate numerical solutions to the full nonlinear PDE based on (1.1) were obtained by Reinelt & Kraynik (1993) using finite difference methods. Large uniaxial extensional deformations of the foam up to the elastic limit were also analysed. The initial foam orientation was chosen with the quadrilateral faces of a Kelvin cell and the principal axes of the extensional deformation aligned with the axes of a Cartesian coordinate system. In this highly symmetric situation, the quadrilateral faces remain flat and the computational domain for the deformed foam is only one quarter of a hexagonal face.

In simple shear, the computational domain is much larger even for those orientations of the foam that have a high degree of symmetry.

Here, the elastic-plastic behaviour of a Kelvin foam is determined for quasi-static simple shearing deformations. Finite rate effects due to viscous flow in thin films are neglected when we compute the evolution of foam structure and effective stress with shear strain. Many topological rearrangements of the connected film network occur during flow. In a Kelvin foam, a surface shared by two bubbles 'disappears' as the bubbles pull apart from each other; at the same time, a new surface 'appears' where two other bubbles come together. We follow Weaire & Kermode (1983) who refer to this topological transition as a T1 in the analogous two-dimensional situation. In two dimensions, a T1 is triggered when an edge length goes smoothly to zero with strain. The corresponding situation in three dimensions – the surface area of a film going smoothly to zero with strain triggering a T1 – does not occur in the complete solutions examined here. By choosing initial orientations of the foam that lead to strain-periodic solutions, the number of unique neighbour-switching transitions is reduced. A second type of topological transition, a T2, refers to an entire bubble disappearing because all of the gas diffuses out. There is no diffusion between identical bubbles with equal pressures; consequently, T2s do not occur in a perfectly ordered foam.

A complete solution is calculated for three different foam orientations. An approximate solution, which we refer to as the minimal planar solution, is calculated for these and other orientations. Reinelt (1993) has determined a planar solution where the dihedral angles between faces remain fixed at their initial values during deformation. In contrast, the dihedral angles vary with deformation in the minimal planar solutions.

The following analysis of simple shearing flow for a dry, perfectly ordered foam extends to three dimensions the seminal two-dimensional analysis of Princen (1983), which was generalized to arbitrary foam orientations by Khan & Armstrong (1986) and Kraynik & Hansen (1986).

Matzke (1946) did not find a single Kelvin cell during meticulous observations of several hundred bubbles in carefully prepared foams that he believed to be monodisperse. The cells in his disorded foams exhibited an impressive variety of topologies. Weaire & Phelan (1994*b*) have observed Kelvin cells but found that the tendency to order is quite limited in bulk foams under normal circumstances. Since real bulk foams are disordered, our analysis is clearly a first step toward understanding foam flow from a microrheological point of view.

2. Evolution of foam structure with shear

2.1. *Undeformed foams*

The bubble centres in an unbounded, undeformed Kelvin foam form a body-centred-cubic (b.c.c.) lattice. A lattice consists of all points

$$\Lambda_m = m_1 \boldsymbol{L}_1 + m_2 \boldsymbol{L}_2 + m_3 \boldsymbol{L}_3 \tag{2.1}$$

where the lattice vectors $\boldsymbol{L}_1$, $\boldsymbol{L}_2$, $\boldsymbol{L}_3$ are linearly independent basis vectors and $\boldsymbol{m} = \{m_1, m_2, m_3\}$ is any set of integers. Initial orientations of the foam are specified by applying rotations to a reference structure, which has a bubble centred at the origin of a Cartesian coordinate system with the vectors normal to the quadrilateral faces of a Kelvin cell aligned with the x-, y-, and z-axes. A set of lattice vectors for

the reference structure is

$$\boldsymbol{L}_1^0 = \frac{V^{1/3}}{2^{2/3}} \begin{bmatrix} 1 \\ 1 \\ 1 \end{bmatrix}, \quad \boldsymbol{L}_2^0 = \frac{V^{1/3}}{2^{2/3}} \begin{bmatrix} 1 \\ 1 \\ -1 \end{bmatrix}, \quad \boldsymbol{L}_3^0 = \frac{V^{1/3}}{2^{2/3}} \begin{bmatrix} 0 \\ 2 \\ 0 \end{bmatrix}, \tag{2.2}$$

where V is the volume of a Kelvin cell. We set $V = 1$ in all calculations which is equivalent to scaling length by $V^{1/3}$.

To get other orientations of the foam, the reference structure is rotated about the y-axis through the angle ϕ, then about the x-axis through the angle θ, and finally about the y-axis through the angle ψ; all rotations are in the counterclockwise direction. The initial lattice vectors of the undeformed foam in the new orientation are given by $\boldsymbol{L}_i^Q = \boldsymbol{Q}\,\boldsymbol{L}_i^0$, where

$$\boldsymbol{Q} = \begin{bmatrix} \cos\psi & 0 & \sin\psi \\ 0 & 1 & 0 \\ -\sin\psi & 0 & \cos\psi \end{bmatrix} \begin{bmatrix} 1 & 0 & 0 \\ 0 & \cos\theta & -\sin\theta \\ 0 & \sin\theta & \cos\theta \end{bmatrix} \begin{bmatrix} \cos\phi & 0 & \sin\phi \\ 0 & 1 & 0 \\ -\sin\phi & 0 & \cos\phi \end{bmatrix} \tag{2.3}$$

is a product of three rotation matrices. There are different conventions for defining the Euler angles given in (2.3); our choice simplifies the classification scheme discussed below.

2.2. *Foam deformation*

For homogeneous deformations, the lattice vectors are given by $\boldsymbol{L}_i = \boldsymbol{F}\,\boldsymbol{L}_i^Q$, where $\boldsymbol{F}$ is the deformation gradient. An undeformed foam with different initial orientations is sheared in the xy-plane with

$$\boldsymbol{F} = \begin{bmatrix} 1 & \gamma & 0 \\ 0 & 1 & 0 \\ 0 & 0 & 1 \end{bmatrix} \tag{2.4}$$

Here, $\gamma = \dot{\gamma}\,t$ is the shear strain, $\dot{\gamma}$ is the shear rate, and t is time.

The strain-periodic orientations of a b.c.c. lattice are classified in the following way. First, we choose values for the angles ϕ and θ so that the lattice points all lie in parallel planes corresponding to $y = i\,\Delta y$, where i is an integer and Δy is the spacing between planes. We order these solutions with decreasing Δy. Second, we choose the angle ψ so that we get a strain-periodic solution. We order these solutions with increasing strain period. Table 1 gives the angles that define the orientations with the smallest strain periods. The orientations labelled 1.x, 2.x, and 3.x have separation distance Δy equal to $V^{1/3}/2^{1/6}$, $V^{1/3}/2^{2/3}$, and $V^{1/3}/(2^{1/6}3^{1/2})$ respectively.

The foam is deformed by increasing the shear strain. At each value of γ, the structure with minimal surface area is computed. The shear strain is increased until a solution that satisfies Plateau's laws cannot be found. This point of instability, an elastic limit, is always associated with shrinking faces, but the area of these faces does not go smoothly to zero with strain. Stability is restored by topological transitions (T1s) that result in a Kelvin foam with different geometry and lower surface area.

2.3. *Topological transitions*

Because of the perfect order and symmetry of a Kelvin foam, there are three basic T1 types; we refer to them as standard, point, and triple transitions (see figure 2). Schwarz (1965) observed and classified topological rearrangements in disordered polyhedral foams. He found standard transitions but no point or triple transitions, which stem from the perfect order of a Kelvin foam.

Orientation	$\tan\phi$	$\tan\theta$	$\tan\psi$	γ_p	$\overline{\sigma}_{xy}$	$\overline{N}_1$	$\overline{N}_2$
1.1	0	1	$1/\sqrt{2}$	$\sqrt{3/2}$	0.0818	0.0451	−0.0623
1.2^t	0	1	∞	$\sqrt{2}$	0.7043	0.8993	−0.5307
1.3^p	0	1	0	2	0.1800	0.0613	−0.2961
1.4	0	1	$3/\sqrt{2}$	$\sqrt{11/2}$	0.1128	0.2029	−0.0347
1.5	0	1	$\sqrt{2}/6$	$\sqrt{19/2}$	0.1579	0.0104	−0.2708
1.6	0	1	$\sqrt{2}$	$\sqrt{12}$	0.1468	0.2133	−0.1128
1.7	0	1	$5/\sqrt{2}$	$\sqrt{27/2}$	0.3299	0.4646	−0.1955
2.1^p	0	0	0	2	0.2242	0.5097	−0.4235
2.2^t	0	0	1	$2\sqrt{2}$	0.4894	1.3606	−0.9200
2.3	0	0	1/2	$2\sqrt{5}$	0.2193	1.0112	−0.7606
3.1^t	1	$1/\sqrt{2}$	0	$3/\sqrt{2}$	0.5298	0.4471	−0.2807
3.2	1	$1/\sqrt{2}$	∞	$2\sqrt{3}$	0.1460	0.8906	−0.5814

TABLE 1. Strain-periodic orientations for simple shear. Orientations that have point (p) or triple (t) transitions are indicated; these initial structures have mirror symmetry about the (x, y)-plane. Minimal planar results: $\overline{\sigma}_{xy}$ is the average shear stress, $\overline{N}_1 = \overline{\sigma}_{xx} - \overline{\sigma}_{yy}$ and $\overline{N}_2 = \overline{\sigma}_{yy} - \overline{\sigma}_{zz}$ are the normal stress differences. The stress scale $T/V^{1/3}$ is the same in all tables.

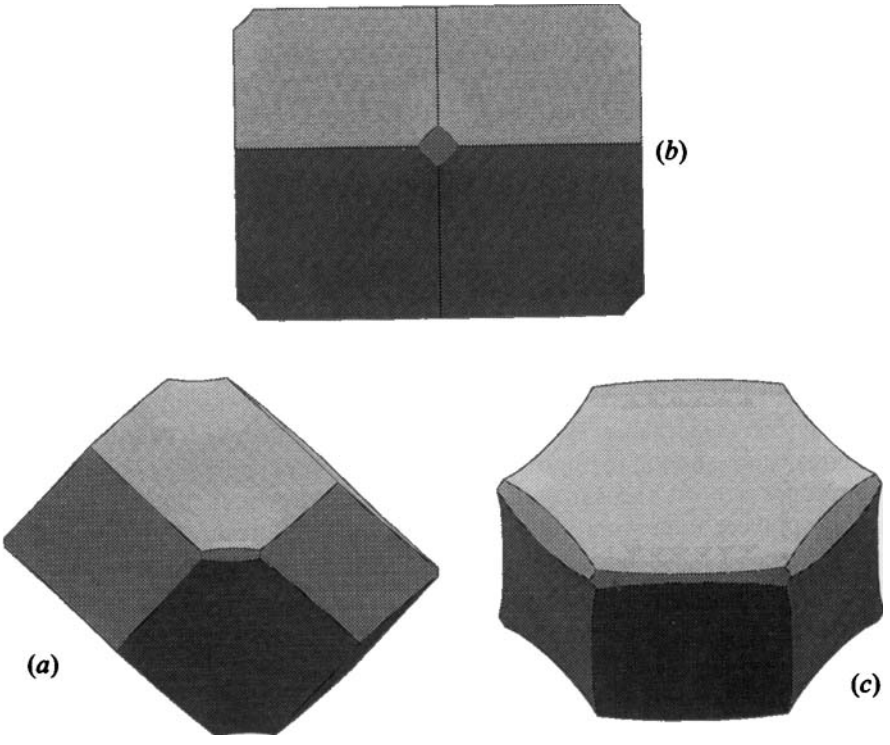

FIGURE 2. Shrinking faces and edges on highly distorted Kelvin cells just prior to the three basic topological transitions: (*a*) standard T1, orientation 1.1, $\gamma = 0.60$, as in figures 3(*c*) and 8(*c*); (*b*) point T1, orientation 1.3, $\gamma = 0.54$, compare with figure 4(*c*); (*c*) triple T1, orientation 1.2, $\gamma = \sqrt{2}$, as in figure 4(*g*). The standard T1 for (*a*) occurs when the short edges go to zero length at $\gamma = 0.617$. The point T1 for (*b*) occurs at $\gamma = 0.548$. The triple T1 for (*c*) occurs when opposite 'long' edges of the shrinking hexagonal face touch when $\gamma = 1.47$.

Before describing the T1 types, it is useful to review geometrical features that are common to all deformed Kelvin foams. A Kelvin cell has 14 faces, 36 edges, and 24 vertices, but all of these features are shared with neighbours so there are only 7 faces, 12 edges, and 6 vertices in a unit cell. The six vertices on a hexagonal face and the twelve edges on three quadrilaterals oriented in different directions are representative. The seven faces that can be seen in figure 1, for example, are representative; those that cannot be seen are redundant. As a consequence of spatial periodicity, the entire foam geometry is determined by translating these representative features through linear combinations of the lattice vectors. The centre of each face is located at the midpoint between two bubble centres and moves affinely with the homogeneous deformation. From symmetry, the centre of each face is also located at the midpoint between opposite vertices; thus, only three of the six representative vertex positions are unique. Furthermore, each face is symmetric about its centre so there are only six unique edge lengths. Each edge is shared by two hexagons and one quadrilateral. In the following description of the T1s, it is useful to keep in mind that the Kelvin cell gains and loses neighbours and faces, and some faces gain or lose edges, but each topological rearrangement just results in a Kelvin cell with different shape. The bubble centres (and therefore, the centre of each face separating old cell neighbours) do not change position during a T1.

Standard transitions occur when one of the six unique edge lengths tends to zero (consult figures 2*a* and 3); the vanishing edge corresponds to opposite edges of a quadrilateral face and opposite edges of two hexagonal faces. The two hexagonal faces become quadrilaterals and the quadrilateral face degenerates to form a 'new' edge. This situation is unstable because Plateau's laws are violated: five different edges meet at each vertex of the 'new' edge instead of the required four; and the 'new' edge is shared by four cells instead of the required three. Two of these cells were neighbours that shared the entire shrinking quadrilateral face; the other two cells were not neighbours. Foam topology consistent with Plateau's laws is restored when the original cell neighbours separate and a 'new' quadrilateral face emerges from the unstable edge. The 'new' face is shared by the new cell neighbours. Two of the original hexagons remain hexagons. It is important to note that the consequences of a standard transition are unique.

Point and triple transitions occur when the foam structure possesses mirror symmetry about the (x, y)-plane and two of the six unique edge lengths tend to zero simultaneously, as shown in figures 2 and 4. A point transition occurs when the shrinking edges are on the same quadrilateral, as shown in figure 2(*b*). Since the lengths of opposite edges are equal, all four edges contract and the quadrilateral tends to a point. The shrinking quadrilateral face in figure 4(*a–c*) is bisected diagonally by the (x, y)-plane. In general, there are two possible standard transitions associated with each quadrilateral face depending on which set of opposite edges vanishes. A point transition requires a choice between these two standard transitions. This choice is not significant because the resulting foam structures are mirror images of each other with respect to the (x, y)-plane, and they have the same stress.

A triple transition occurs when the shrinking edges are on different quadrilaterals. This can happen when a quadrilateral face is bisected crosswise by the (x, y)-plane, as shown in figures 2(*c*) and 4(*e–h*). Two of the unique quadrilateral faces are mirror images of each other. As the foam is strained, opposite sides of these quadrilaterals and four sides of a hexagonal face all tend to zero length. As a consequence, three of the seven unique faces shrink simultaneously and all three corresponding cell neighbours are lost, which motivitated us to call this a triple transition. For

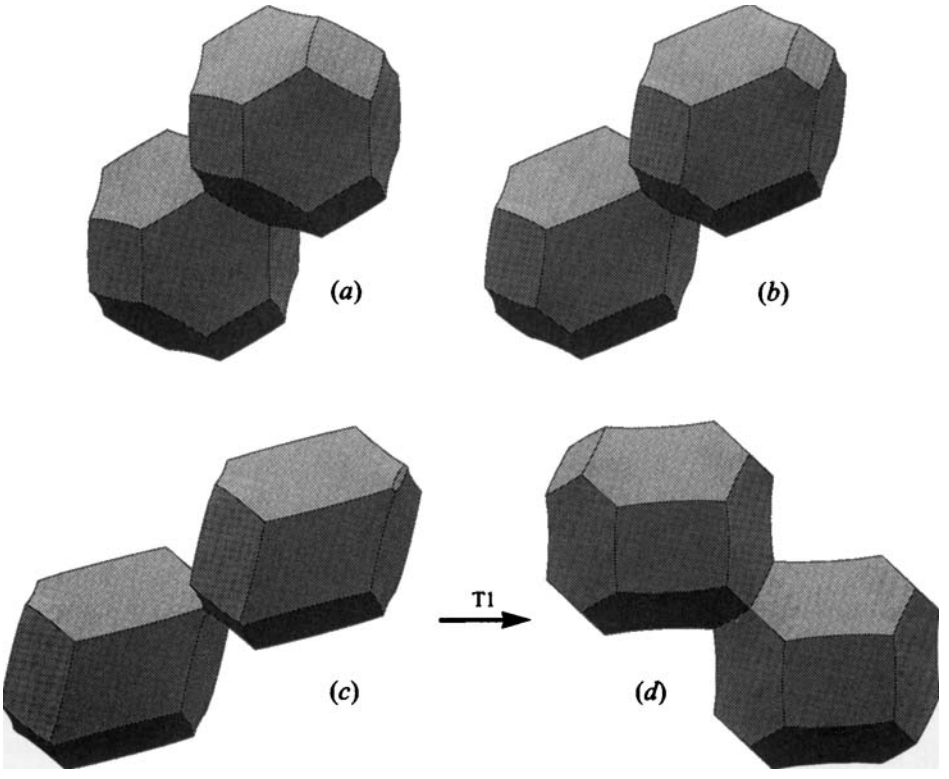

FIGURE 3. Standard topological transition for orientation 1.1 with (*a*) $\gamma = 0$, (*b*) 0.30, (*c*) 0.60, and (*d*) 0.62. Cell neighbours in (*a*), (*b*), and (*c*) share the quadrilateral face that shrinks as γ increases. The T1 occurs when opposite edges of the quadrilateral face go to zero length at $\gamma = 0.617$; original cell neighbours separate and a 'new' face forms between the new neighbours in (*d*). Each Kelvin cell is shown from a slightly different viewing angle in figure 8. The view of (*c*) is also different in figure 2(*a*).

some orientations that are not shown, the quadrilateral crossing the (x, y)-plane has a shrinking edge and there is a standard transition. Further details about the orientations and transitions are given in Reinelt (1993).

3. Macroscopic stress

The instantaneous macroscopic stress tensor $\boldsymbol{\sigma}$ for the foam is calculated by averaging the local stress over the unit cell. Reinelt & Kraynik (1993) evaluated the stress for a Kelvin foam under static conditions by accounting for all seven unique faces of a deformed Kelvin cell and obtained

$$\boldsymbol{\sigma} = -p_b \boldsymbol{I} + \frac{2T}{V} \sum_{k=1}^{7} \int\int_{S_k} (\boldsymbol{I} - \boldsymbol{n}_k \boldsymbol{n}_k^t) \, \mathrm{d}A \tag{3.1}$$

where p_b is the pressure inside each bubble, T is surface tension, V is the bubble volume, $\boldsymbol{I}$ is the identity matrix, $\boldsymbol{n}_k$ is a unit vector normal to the kth face, $\boldsymbol{n}_k^t$ is the transpose of $\boldsymbol{n}_k$, and $\mathrm{d}A$ is the differential area element. Since each film has two interfaces, the film tension is $2T$. The shear stress σ_{xy} can be evaluated using (3.1) or

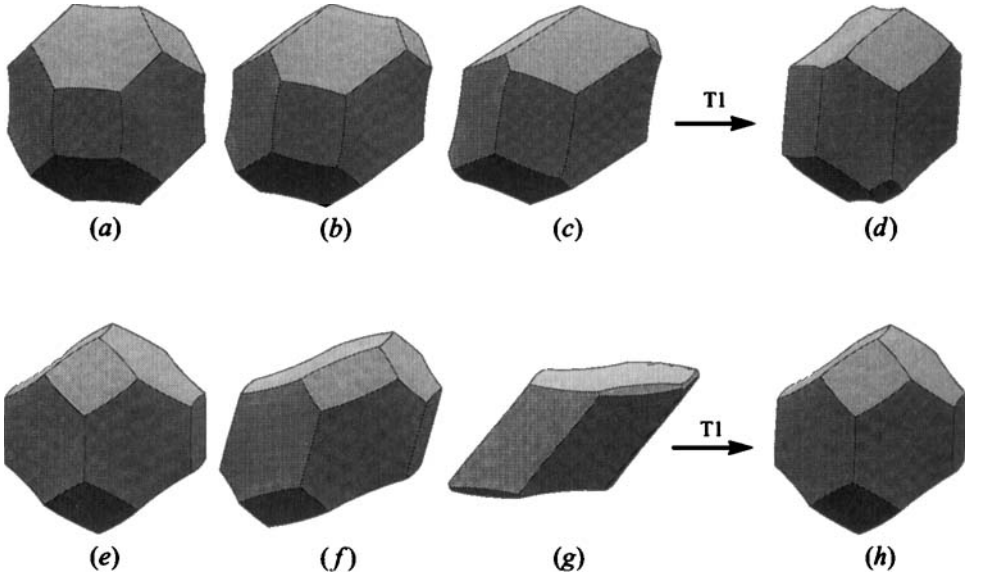

FIGURE 4. Evolution of foam geometry with strain for orientation 1.3 with (*a*) $\gamma = 0$, (*b*) 0.30, (*c*) 0.50, just before a point transition, and (*d*) 0.55; and orientation 1.2 with (*e*) $\gamma = 0$, (*f*) 0.50, (*g*) $\sqrt{2}$, just before a triple transition, and (*h*) 1.50. Topological transitions as in figures 2(*b*) and 2(*c*). Viewing angle as in figure 3.

it can be evaluated from the surface energy using

$$\sigma_{xy} = \frac{\mathrm{d}}{\mathrm{d}\gamma}\left(\frac{2\,TS}{V}\right) = \frac{2\,T}{V}\,\frac{\mathrm{d}}{\mathrm{d}\gamma}\sum_{k=1}^{7} S_k\,. \tag{3.2}$$

Here, S is the total surface area of a bubble and S_k refers to the kth interface. Our calculations using the two methods give consistent results.

The shear modulus G is the initial slope of the stress–strain curve. The cubic symmetry of an undeformed Kelvin foam implies anisotropic linear elastic behaviour with two independent shear constants (Love 1944; Nye 1985), which we label G_{min} and G_{max}. These labels anticipate our results because symmetry alone does not give the relative magnitude of the two positive constants. Cubic symmetry gives the orientation dependence of the shear modulus as

$$G = G_{max} + 2\,(G_{min} - G_{max})(Q_{11}^2 Q_{21}^2 + Q_{12}^2 Q_{22}^2 + Q_{13}^2 Q_{23}^2) \tag{3.3}$$

where Q_{ij} are matrix elements given in (2.3). An average shear modulus $\overline{G}$ is defined by integrating over all possible orientations of the foam

$$\overline{G} = \frac{1}{8\pi^2}\int_0^{2\pi}\int_0^{\pi}\int_0^{2\pi} G\,\sin\theta\,\mathrm{d}\phi\,\mathrm{d}\theta\,\mathrm{d}\psi = \tfrac{2}{5}\,G_{min} + \tfrac{3}{5}\,G_{max}\,. \tag{3.4}$$

For spatially periodic foams, viscometric functions are evaluated by averaging the instantaneous stress over time. When the foam structure and stress are periodic with strain

$$\overline{\boldsymbol{\sigma}} = \frac{1}{\gamma_p}\int_{\gamma}^{\gamma+\gamma_p} \boldsymbol{\sigma}\,\mathrm{d}\gamma, \tag{3.5}$$

where $\boldsymbol{\sigma}$ is the instantaneous stress given in (3.1), $\overline{\boldsymbol{\sigma}}$ is the time-average stress, and γ_p

	G_{min}	G_{max}	$\overline{G}$
Complete solution	0.5706	0.9646	0.8070
Minimal planar solution	0.55254	0.96965	0.80281
Fixed-angle solution (energy)	0.60952	0.97788	0.83054
Fixed-angle solution (force)	0.79370	0.91649	0.86737

TABLE 2. The shear moduli were calculated using the force and energy methods, which correspond to (3.1) and (3.2) respectively. The two methods agree for the complete solution as expected. They also agree for the minimal planar solution, which is not expected. The two methods give very different results for the planar solution with fixed dihedral angles.

is the strain period. The time-average shear stress can also be evaluated from σ_{xy} in (3.2). This average includes contributions from all intermediate foam structures and removes the explicit dependence on time associated with a spatially periodic model.

4. Results

4.1. *Minimal planar solution*

Before solving the complete minimal surface problem, we develop an approximate solution that assumes planar faces. In previous analyses, Reinelt & Kraynik (1993) and Reinelt (1993) assumed that the dihedral angle between faces remains constant during deformation. The two dihedral angles of a regular tetrakaidecahedron are 109.47° and 125.26°; equilibrium requires 120°, which of course cannot be satisfied by flat faces. Here, we relax the constant-angle condition and seek the planar solution at each value of strain that has minimal surface area.

As discussed above, the centre of each face moves affinely with the homogeneous deformation and there are three unique vertices to determine. The two diagonals through the midpoint of a quadrilateral face specify a plane and its normal. The three diagonals through the midpoint of a hexagonal face do not necessarily lie in the same plane. Requiring these diagonals to be coplanar provides a constraint for each of the four hexagonal faces. For each set of face centres, the objective is to minimize the total surface area of the foam as a function of the nine coordinates that specify the three unique vertices subject to the four constraints.

Table 2 lists the minimum, maximum, and average shear moduli for the minimal planar solution. For orientation 1.x, the shear modulus in (3.3) reduces to $G = G_{max} + (G_{min} - G_{max}) \sin^2 \psi$. The maximum value is calculated from orientation 1.2 and the minimum value is calculated from orientation 1.3 (see table 1). The shear modulus for orientations 2.x and 3.x are $G = G_{max}$ and $G = G_{max} + (G_{min} - G_{max})(1 + \sin^2 \psi)/3$ respectively.

For comparison, the shear modulus is also given for the complete solution discussed in the next section and for the planar solution with constant dihedral angles. Note that the approximate solutions do not provide an upper bound on the shear modulus; G_{min} for the minimal planar solution is lower than the corresponding value for the complete solution. It is possible for this to occur because the initial structures for the approximate and complete solutions are not the same. Agreement between the shear stress calculated from the force and energy methods does not necessarily imply that an accurate value of the shear stress has been determined. The two methods agree to five decimal places for the minimal planar solution, but the results differ from

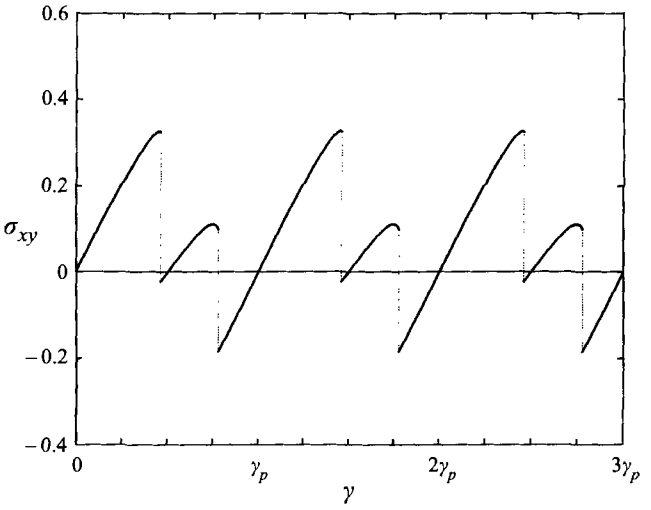

FIGURE 5. Shear stress σ_{xy} as a function of γ for orientation 1.1, minimal planar solution. The stress scale $T/V^{1/3}$ is the same in all figures.

the complete solution in the second decimal place. The minimal planar solution is superior to the planar solution with constant dihedral angles.

Figure 5 shows the instantaneous shear stress for orientation 1.1 which has the smallest strain period. This orientation has two standard transitions. In each of these transitions one of the six edge lengths tends to zero continuously with increasing shear strain. Since this is a planar model, the area of the quadrilateral face also tends to zero continuously with strain and vanishes to a line segment. The Kelvin cells form layers with bubble centres in planes of constant y. At the end of each strain period the cells have shifted position relative to the layer above and below. The instantaneous normal stress differences, $N_1 = \sigma_{xx} - \sigma_{yy}$ and $N_2 = \sigma_{yy} - \sigma_{zz}$, are shown in figure 6. The time-average stresses are given in table 1.

There is a second type of standard transition in which an edge length does not tend to zero continuously with strain. Approximately 20% of the transitions for the orientations in table 1 are of this type. Just before the transition the shrinking edge length is small but finite, ranging from 0.6% to 7.3% of that in an undeformed foam. With a very small increase in strain (10^{-5} for minimal planar solutions) the edge length drops to zero triggering a T1. This is reminiscent of behaviour near the turning point calculated by Reinelt & Kraynik (1993) for large uniaxial extension of a Kelvin foam.

For orientation 1.2, there is one triple transition per cycle. In the minimal planar solution, two of the six edge lengths and the area of three of the seven faces tend to zero continuously with strain. The first transition occurs when γ is greater than γ_p, so the foam never returns to its undeformed structure during simple shearing flow. The shear stress at a triple transition tends to be higher than it is for a standard transition. Note that the three orientations in table 1 that have triple transitions also have the three highest values of $\bar{\sigma}_{xy}$. As discussed by Reinelt (1993), the (x, y)-planar cross-section of an orientation with triple transitions is similar to a perfectly ordered two-dimensional foam, which has hexagonal cells. The results for orientations with triple transitions are significantly different from other cases. Clearly, it is not prudent to draw conclusions from a single orientation of a Kelvin foam.

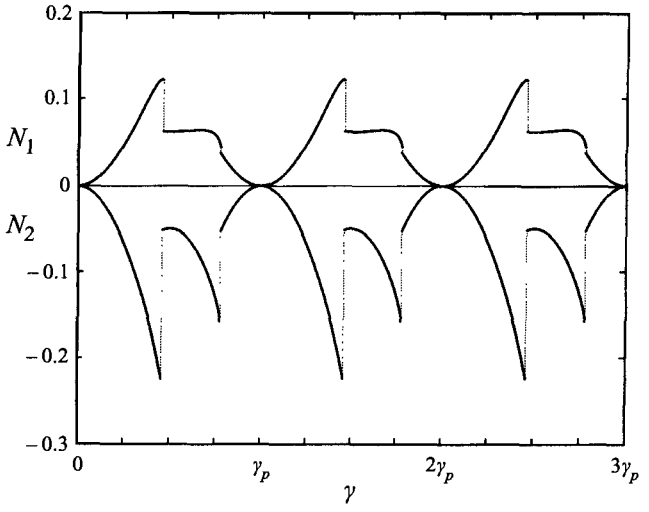

FIGURE 6. Normal stress differences $N_1 = \sigma_{xx} - \sigma_{yy}$ and $N_2 = \sigma_{yy} - \sigma_{zz}$ as a function of γ for orientation 1.1, minimal planar solution.

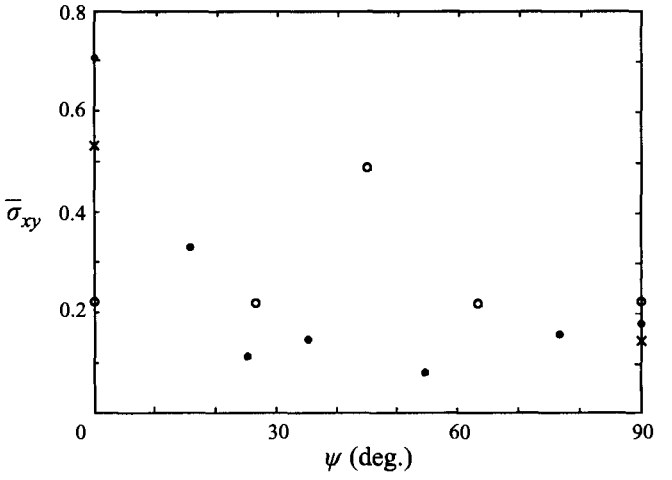

FIGURE 7. Time-average shear stress $\bar{\sigma}_{xy}$ versus orientation angle ψ for orientations 1.x, 2.x, and 3.x: •, orientation 1.x; ○, orientation 2.x; ×, orientation 3.x. Extra data points for orientation 2.x are plotted because this orientation is symmetric about $\psi = 45°$. The largest three values shown correspond to orientations with triple transitions.

Figure 7 shows $\bar{\sigma}_{xy}$ for different orientation angles ψ. Even though all of the results have been plotted on a single graph, there is no significant relationship between the values of ψ for the three different classes, 1.x, 2.x, and 3.x.

4.2. *Complete solution*

The Kelvin cell with minimal surface area shown in figure 1 represents the shape of each bubble in an undeformed perfectly ordered foam, where each cell sits on a b.c.c. lattice. Brakke (1977, 1992, 1995) has computed the geometry of a Kelvin foam with his Surface Evolver program, which converges to a minimal surface by simulating the process of evolution by mean curvature. We have used the Surface Evolver to

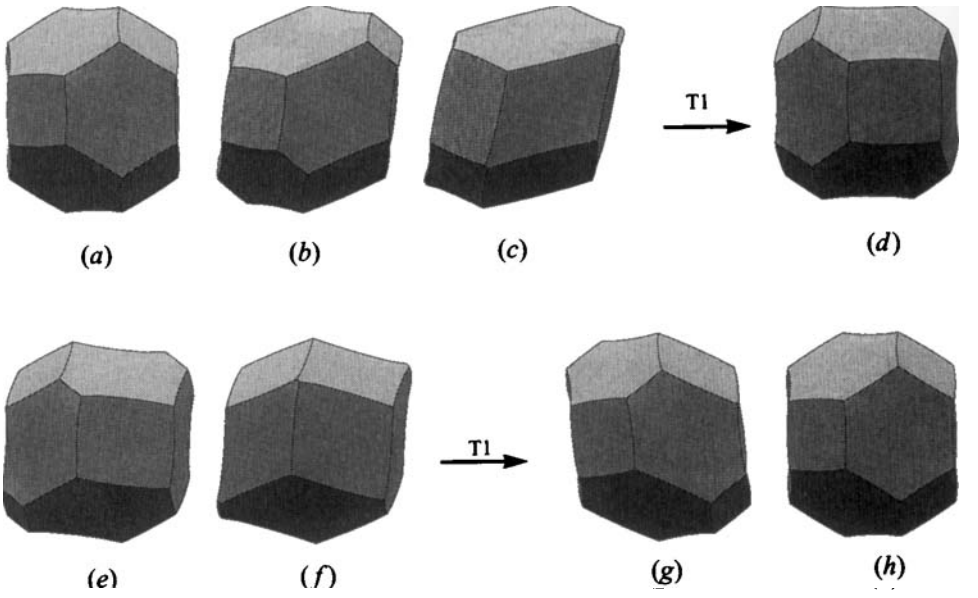

FIGURE 8. Evolution of foam geometry with strain for orientation 1.1, which has the smallest strain period $\gamma_p = \sqrt{3/2}$. (*a*) $\gamma = 0$, (*b*) 0.30, (*c*) 0.60, (*d*) 0.62, (*e*) 0.80, (*f*) 0.99, (*g*) 1, and (*h*) γ_p. Standard topological transitions occur when opposite edges of shrinking quadrilateral faces go to zero length at $\gamma = 0.617$ and $\gamma = 0.998$. The Kelvin cells in (*a*) and (*h*) have identical shape but some neighbours are different as a consequence of the T1s. All views are along the z-axis; this is slightly different from figure 3, which contains different views of (*a–d*).

analyse large extensional deformations of a Kelvin foam, the problem originally solved by Reinelt & Kraynik (1993) using finite difference methods. The Surface Evolver and finite difference results are in agreement. We have also used the Surface Evolver to compute the results reported here. To determine the shape of the curved surfaces, each face is subdivided with triangular facets. Each n-sided face normally has $4^{\mathscr{R}}n$ facets, where $\mathscr{R}$ is the level of refinement. We typically use $\mathscr{R} = 3$, e.g. each hexagonal face has 384 facets. The shape of each facet surface can be represented by a linear function, giving flat facets, or by a quadratic function, which improves accuracy. As the foam is deformed by increasing γ we reduce the number of facets on faces that shrink; this improves convergence of the calculation. Available computer memory and speed permit the use of quadratic facets and $\mathscr{R} = 5$ to verify the accuracy of our computations.

The Surface Evolver was used to compute complete solutions for the first three orientations in table 1. Figure 8 shows the evolution of foam structure for orientation 1.1. The edges of the quadrilateral faces bow out so that they meet at the tetrahedral angle. When a quadrilateral face shrinks with increasing strain, one of the six unique edge lengths tends to zero continuously with strain, but the area of the quadrilateral face remains finite (see figures 2*a* and 3). When an edge vanishes, the foam structure is unstable and the shrinking face disappears as part of the standard T1 discussed above. Figure 9(*a–c*) shows the instantaneous shear stress for the complete and minimal planar solutions for orientations 1.1, 1.2, and 1.3.

For orientations 1.1 and 1.3, the transitions for the complete solution are slightly delayed when compared to the minimal planar solution, and the time-average shear stress is higher for the complete solution.

Orientation 1.2 only has a single triple transition per cycle. A hexagon and two

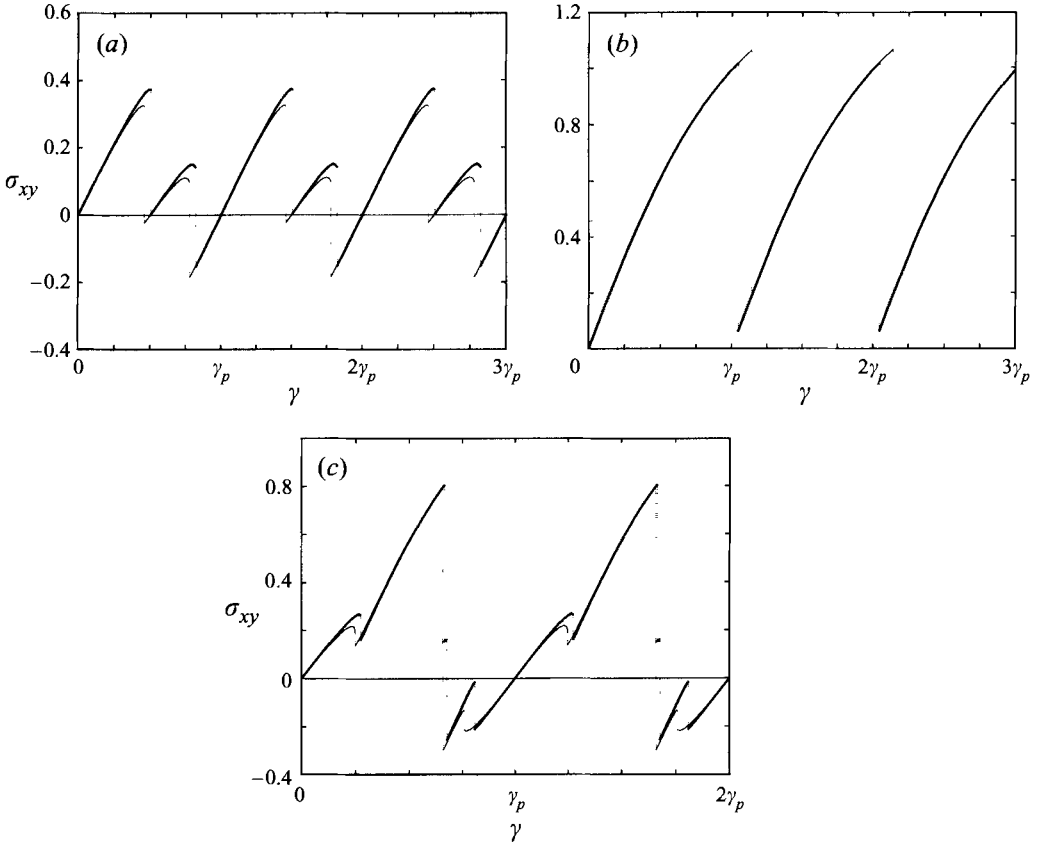

FIGURE 9. Shear stress σ_{xy} versus γ for orientations (*a*) 1.1, (*b*) 1.2 and (*c*) 1.3. ——, complete solution; ——, minimal planar solution. The periods are $\gamma_p = \sqrt{3/2}, \sqrt{2}$, and 2 as given in table 1.

quadrilaterals shrink simultaneously, as shown in figures 2(*c*) and 4(*e–h*). Opposite edges of the shrinking hexagon that are not contracting bow in and eventually touch at their centre triggering a T1. This transition precedes the corresponding minimal planar transition and the time-average shear stress is smaller for the complete solution. All edge lengths and face areas are finite when this triple transition is initiated.

For orientation 1.3, the first transition is a point transition of the turning point type; the four equal edge lengths of the shrinking quadrilateral face are small but finite, as shown in figures 2(*c*) and 4(*a–d*). The next two are standard transitions with an edge length tending to zero continuously. The last transition is a standard transition of the turning point type.

Table 3 shows the time-average viscometric functions. The results for $\overline{\sigma}_{xy}$ are graphed in figure 10 along with the minimal planar results for orientations 1.*x*. The time-average normal stress differences are graphed in figure 11. The difference between minimal planar and complete solutions for a given orientation are much smaller than the variation between different orientations. For this reason, we do not calculate the complete solution for all the different orientations shown in table 1. Clearly, finding an accurate solution to the complete problem at each value of strain is much more computationally intensive than determining the minimal planar solution.

Orientation	$\bar{\sigma}_{xy}$	$\bar{N}_1$	$\bar{N}_2$
1.1	0.1191	0.0535	−0.0705
1.2^t	0.6168	0.7154	−0.4182
1.3^p	0.2040	0.0644	−0.3058

TABLE 3. Complete solutions: $\bar{\sigma}_{xy}$ is the average shear stress, $\bar{N}_1 = \bar{\sigma}_{xx} - \bar{\sigma}_{yy}$ and $\bar{N}_2 = \bar{\sigma}_{yy} - \bar{\sigma}_{zz}$ are the normal stress differences. Point (p) and triple (t) transitions are indicated.

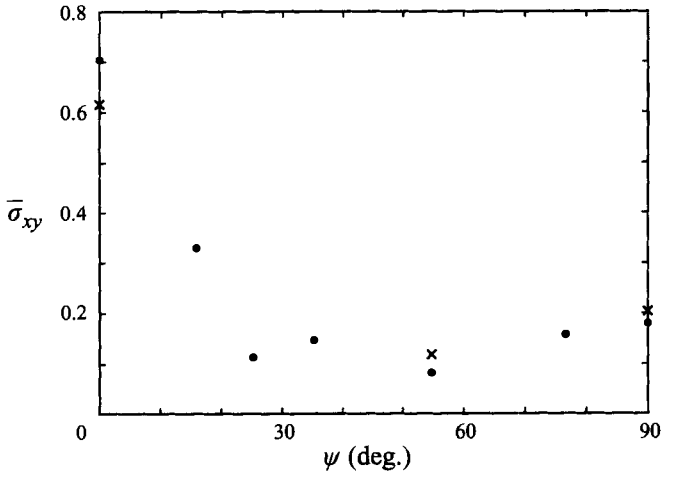

FIGURE 10. Time-average shear stress $\bar{\sigma}_{xy}$ versus orientation angle ψ for orientations 1.x: •, minimal planar solution; ×, complete solution.

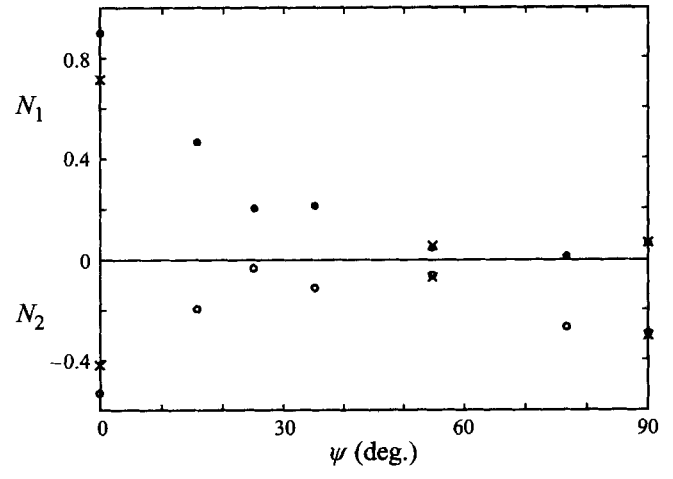

FIGURE 11. Time-average normal stress differences $N_1 = \sigma_{xx} - \sigma_{yy}$ and $N_2 = \sigma_{yy} - \sigma_{zz}$ versus orientation angle ψ for orientation 1.x: •, N_1 minimal planar solution; ○, N_2 minimal planar solution; ×, complete solution.

5. Comparison with experiments and discussion

As discussed in the introduction, topological transitions in dry, two-dimensional foams are triggered by an edge length going to zero continuously with strain. The analogous three-dimensional event – the area of a face tending to zero continuously with strain triggering a T1 – does not occur. In a Kelvin foam, a T1 is triggered by an edge length going to zero, a turning point where an edge length is small, or opposite edges of a hexagonal face touching each other. The last situation only occurs for highly symmetric orientations of a Kelvin foam and is unlikely to occur in disordered foams.

Princen & Kiss (1986) have measured the static shear modulus of a series of concentrated oil-in-water emulsions with polydisperse drop-size distributions. By taking the limit as $\Phi \to 1$, where Φ is the volume fraction of the disperse phase, their result becomes $G = 0.509\ T/R_{32}$, where R_{32} is the surface-volume mean drop radius that characterizes spherical drops in emulsions diluted with excess water.

For a Kelvin foam, R_{32} is calculated from $V = (4/3)\pi R_{32}^3$. In units of T/R_{32}, the shear moduli for the complete solution lie in the range $0.354 < G < 0.598$ with an orientation-average of 0.500. The shear moduli for the minimal planar solution satisfy $0.343 < G < 0.602$ with an average of 0.498. The average shear moduli agree quite well with the empirical correlation.

The dynamic (or viscometric) yield stress $\bar{\sigma}_{xy}$ for dry foams is a direct result of the frequency and magnitude of the energy jumps associated with topological transitions. In fact, using the energy method, the shear stress integrated over a strain period is exactly the difference in surface energy summed over all of the jumps. This connection between energy jumps and dynamic yield stress was recognized by Bonnecaze & Brady (1992) for electrorheological fluids and Okuzono, Kawasaki & Nagai (1993) for two-dimensional random foams.

Princen (1985) measured the yield stress for highly concentrated emulsions and obtained F_{max} in the semi-empirical relation $\bar{\sigma}_{xy} = 1.277\ (T/R_{32})\ \Phi^{1/3} F_{max}(\Phi)$. It is difficult to extrapolate the experimental data for F_{max} to $\Phi = 1$ (dry foams) for two reasons: first, F_{max} increases rapidly as $\Phi \to 1$; second, there are different curves for F_{max} depending on whether the actual film thickness in the experiments was 0.00, 0.05, or 0.10 μm. There is considerable variation between the extrapolated values for the three different curves. For reference, the last data point on the curve for zero film thickness is $F_{max} \approx 0.1$ and $\bar{\sigma}_{xy} \approx 0.13\ T/R_{32}$ at $\Phi \approx 0.97$.

The results for the minimal planar solution satisfy $0.0818\ T/V^{1/3} = 0.0507\ T/R_{32} \leqslant \bar{\sigma}_{xy} \leqslant 0.4369\ T/R_{32} = 0.7043\ T/V^{1/3}$. If the three orientations with triple transitions are eliminated, then the top of the range is reduced by a factor of 2 to $0.2047\ T/R_{32}$. For the complete problem, $\bar{\sigma}_{xy} = 0.074$, 0.383, and $0.127\ T/R_{32}$ for orientations 1.1, 1.2, and 1.3.

The time-average shear stress of a Kelvin foam exhibits strong dependence on orientation – much stronger than the shear modulus, which varies by a factor of 2. This demonstrates the importance of examining orientation effects. Orientation dependence, which stems from perfect order and strong symmetry in a Kelvin foam, will decrease with increasing $\mathcal{N}$, the number of distinct bubbles with different shape in the unit cell. A disordered foam has isotropic rheological behaviour. The shortcomings of a Kelvin foam motivate examination of foam structures with large $\mathcal{N}$. Weaire & Phelan (1994*a*) have described a structure with eight bubbles and smaller surface area than a Kelvin cell. Kraynik & Reinelt (1996) have shown that orientation dependence of the shear modulus is an order of magnitude smaller for a Weaire–Phelan foam.

This structure is one of 24 known tetrahedrally close-packed (t.c.p.) crystal structures that contain from 6 to 228 'bubbles' per unit cell (Rivier 1994). Foam geometries based on t.c.p. structures provide many candidates for investigating the microrheology of foams. The rheology of large t.c.p. foams is undoubtedly more representative of real bulk foams than a Kelvin cell.

We thank Ken Brakke for developing and maintaining the Surface Evolver. D.A.R. was supported by National Science Foundation Grant #CTS-9113907. A.M.K. performed this work at Sandia National Laboratories with support from the US Department of Energy under contract #DE-AC04-94AL85000.

REFERENCES

ALMGREN, F. & TAYLOR, J. 1976 The geometry of soap films and soap bubbles. *Sci. Am.* July, 82–93.

BONNECAZE, R. T. & BRADY, J. F. 1992 Yield stresses in electrorheological fluids. *J. Rheol.* **36**, 73–115.

BRAKKE, K. 1977 *The Motion of a Surface by Its Mean Curvature*. Princeton University Press.

BRAKKE, K. A. 1992 The surface evolver. *Exp. Maths* **1**, 141–165.

BRAKKE, K. A. 1995 *Surface Evolver Manual* version 1.98, March.

KELVIN, LORD (THOMPSON, W.) 1887 On the division of space with minimum partitional area. *Phil. Mag.* **24**, 503–514.

KHAN, S. A. & ARMSTRONG, R. C. 1986 Rheology of foams. I. Theory for dry foams. *J. Non-Newtonian Fluid Mech.* **22**, 1–22.

KRAYNIK, A. M. 1988 Foam flows. *Ann. Rev. Fluid Mech.* **20**, 325–357.

KRAYNIK, A. M. & HANSEN, M. G. 1986 Foam and emulsion rheology: A quasistatic model for large deformations of spatially periodic cells. *J. Rheol.* **30**, 409–439.

KRAYNIK, A. M. & REINELT, D. A. 1996 The linear elastic behavior of dry soap foams. *J. Colloid Interface Sci.* Submitted.

LOVE, A. E. H. 1944 *A Treatise on the Mathematical Theory of Elasticity*. Dover.

MATZKE, E. B. 1946 The three-dimensional shape of bubbles in foam–an analysis of the role of surface forces in three-dimensional cell shape determination. *Am. J. Botany* **33**, 58–80.

NYE, J. F. 1985 *Physical Properties of Crystals*. Clarendon Press.

OKUZONO, T., KAWASAKI, K. & NAGAI, T. 1993 Rheology of random foams. *J. Rheol.* **37**, 571–586.

PLATEAU, J. A. F. 1873 *Statique Experimentale et Theorique des Liquides Soumis aux Seules Forces Moleculaires*. Gauthier-Villiard.

PRINCEN, H. M. 1983 Rheology of foams and highly concentrated emulsions. I. Elastic properties and yield stress of a cylindrical model system. *J. Colloid Interface Sci.* **91**, 160–175.

PRINCEN, H. M. 1985 Rheology of foams and highly concentrated emulsions. II. Experimental study of the yield stress and wall effects for concentrated oil-in-water emulsions. *J. Colloid Interface Sci.* **105**, 150–171.

PRINCEN, H. M. & KISS, A. D. 1986 Rheology of foams and highly concentrated emulsions. III. Static shear modulus. *J. Colloid Interface Sci.* **112**, 427–437.

REINELT, D. A. 1993 Simple shearing flow of three-dimensional foams and highly concentrated emulsions with planar films. *J. Rheol.* **37**, 1117–1139.

REINELT, D. A. & KRAYNIK, A. M. 1993 Large elastic deformations of three-dimensional foams and highly concentrated emulsions. *J. Colloid Interface Sci.* **159**, 460–470.

RIVIER, N. 1994 Kelvin's conjecture on minimal froths and the counter-example of Weaire and Phelan. *Phil. Mag. Lett.* **69**, 297–303.

SCHWARZ, H. W. 1965 Rearrangements in polyhedric foam. *Recueil* **84**, 771–781.

TAYLOR, J. E. 1976 The structure of singularities in soap-bubble-like and soap-film-like minimal surfaces. *Ann. Maths* **103**, 489–539.

WEAIRE, D. & KERMODE, J. P. 1983 Computer simulation of a two-dimensional soap froth. *Phil. Mag.* B **48**, 245–259.

WEAIRE, D. & PHELAN, R. 1994*a* A counter-example to Kelvin's conjecture on minimal surfaces. *Phil. Mag. Lett.* **69**, 107–110.

WEAIRE, D. & PHELAN, R. 1994*b* The structure of monodisperse foam. *Phil. Mag. Lett.* **70**, 345–350.